Abstract

Gamma Spectroscopy-based Inverse Radiation Transport Problem Stability Analysis

David Anderson and John Mattingly
North Carolina State University

Inverse radiation transport may be used to characterize unknown radiation sources by estimating properties of the source term and transport medium based on radiation measurements. The inverse radiation transport problem comprises a number of variable parameters, such as source size, shape and geometric configuration, source composition and density, and shielding. The forward radiation transport engine consists of a deterministic transport solver and a detector response function, which together predict the detector response given the problem parameters. A nonlinear optimization routine modifies the transport model parameters to minimize the error between the calculated detector response and the measurement. Various combinations of radiation transport solvers, detector response functions, and optimization methods have previously been explored. Solutions based solely on full-energy peaks in gamma spectroscopic measurements (i.e., on the uncollided gamma leakage) have exhibited multiple possible solutions. It was previously shown that analyzing spectral features resulting from both uncollided and scattered gammas (i.e., photopeaks and Compton continua) resulted in a more constrained solution, relative to a solution obtained from photopeak analysis alone. This paper compares solutions using with an idealized full gamma spectrum to solutions with a gamma spectrum that includes random Poisson noise in the measured spectrum to evaluate the stability of the solution in a more realistic, field type setting. Results are presented that compare the solution stability of the two methods and the sensitivity of each to changes in problem parameters.

Gamma Spectroscopy-based Inverse Radiation Transport Problem Stability Analysis

David Anderson and John Mattingly

Dept. of Nuclear Engineering, North Carolina State University, Burlington Engineering Labs, 2500 Stinson Drive, Raleigh, NC 2760, david_anderson@ncsu.edu, john_mattingly@ncsu.edu

INTRODUCTION

Inverse radiation transport may be used to characterize unknown radiation sources by estimating properties of the source term and transport medium based on measurements of the radiation field. A typical inverse radiation transport problem may include a number of variable parameters, such as source size, shape and geometric configuration, source composition and density, and shielding. In our application, the forward radiation transport engine consists of a deterministic transport solver that predicts the uncollided flux given the problem parameters. A nonlinear optimization routine modifies the transport model parameters to minimize the error between calculated detector response and measurement. Various combinations of radiation transport solvers, detectors, and optimization methods have been explored in previous work [1]-[4]. Solutions based solely on photopeaks in gamma spectroscopic measurements (i.e., on the uncollided gamma leakage) have exhibited multiple possible solutions, where multiple parameter values have equal probability (equal minimum error). Previous analyses [5] showed that a more detailed source model and the addition of spectral features resulting from both uncollided and scattered gammas (i.e., photopeaks and Compton continua) resulted in a more constrained solution relative to a solution obtained from photopeak analysis alone. Solutions using a full gamma spectrum without Poisson distributed noise have since been compared to solutions with a gamma spectrum that includes random Poisson distributed noise in the simulated experimental spectrum to evaluate the stability of the solution in a more realistic, field type setting. Results of analyses using an exhaustive search of the solution parameters, a mesh adaptive direct search (MADS), and Markov Chain Monte Carlo are presented that compare the solution stability of the methods and the sensitivity of each to changes in problem parameters.

PRELIMINARY CALCULATIONS

A ray-trace application was developed in python based on the formulation described by Favorite [6]. The ray trace application calculates the uncollided flux at a point detector from discrete gamma energies, along a line of sight from the point detector back through the source. The LLNL HEU sphere was selected for analysis. The LLNL HEU sphere is well documented [7], and there are experimental test results available which may prove useful for possible later analyses beyond the scope of this paper. The sphere has a 3.151cm outer radius, and is composed of 94.5% enriched uranium. There is a 2.83cm deep conic frustrum void section. For the ray-trace calculation, the volume of this void was modeled as an equal volume spherical void of 1.60cm outer radius. The outer radius of the 1-D sphere was modeled at 3.151cm. Calculations were performed comparing leakage at a distant detector from the MCNP5 model and compared to the leakage calculated by the ray trace application that verified that the LLNL HEU sphere could be accurately modeled as a 1-D sphere [5]. Figure 1 shows the 3D MCNP5 model and a representation of the 1D ray-trace model.

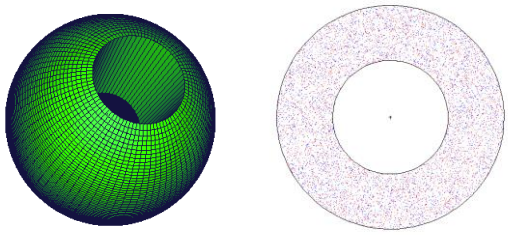

Fig. 1. LLNL HEU sphere, 3D MCNP5 model (left), 1D ray trace model (right)

To characterize the solutions for the hollow sphere, an optimization routine was developed in python that used the SciPy least squares optimization routine scipy.optimize.leastsq [8]. A calculation of gamma leakage at a detector was made at discrete increments of both outer radius and source region thickness for the hollow sphere. Chi-squared error was calculated as the difference between the leakage calculated from the ray trace application and simulated experimental leakage values,

represented by an MCNP5 calculation of the leakage calculated at the actual outer radius and source region thickness, as shown in Equation (1). Since there are four photopeaks in the source model, the chi-squared error is summed and divided by the number of photopeaks.

$$C^2 = \frac{1}{4}\sum_{i=1}^{4} (I_i^{mcnp} - I_i^{rayTrace})^2 / I_i^{mcnp} \quad (1)$$

where:

$C^2 = Chi\text{-}squared\ error$

$i = gamma\ source\ line$

$I_i^{mcnp} = leakage\ flux\ from\ MCNP$

$I_i^{rayTrace} = leakage\ flux\ from\ RayTrace$

EXHAUSTIVE SEARCH

An analysis using a gamma source specified as the four major gamma lines of uranium at 144keV, 186keV, 766keV and 1001keV at 94.5% enrichment did not determine a unique solution, due to the self-shielding in the source region. The four gamma energies have short mean free paths in uranium metal and very few uncollided gammas reach the detector from deep in the source region. With a highly enriched uranium source such as the LLNL sphere, the magnitude of the gammas from ^{238}U, which are the 766keV and 1001keV gammas, are approximately three orders of magnitude lower than the magnitude of the 144kev and 186keV gammas. Therefore the solution is heavily dependent on the two lower gamma energies which have the shorter mean free paths. Mean free paths for the four gamma energies in the source model are given in Table 1, as calculated from the NIST XCOM Cross Section Database [9]

Table 1 – Mean free path in uranium metal

Gamma Energy(keV)	Mean Free Path(cm)
144.0	0.0187
186.0	0.0347
766.0	0.4809
1001.0	0.6780

The left hand plot Figure 2 displays the chi-squared error for each combination of outer radius and source region thickness. The optimization routine determined a value of 3.15cm for the outer radius at each increment of inner radius, however, the horizontal minimum of the 3-D curve displays a continuum of solutions for source region thickness, with each value of source thickness (and therefore inner radius) having the same minimum chi-squared error. ORIGEN [10] was used to create a more detailed source model to determine if additional gamma source lines would contribute to a more constrained solution relative to the simpler 4-line source model. The ORIGEN source contained 1245 gamma lines, and was specified as 94.5% enriched uranium with a twenty year decay time. Source lines above 1001keV were eliminated from the ORIGEN source to enable a direct comparison to the results with the 4-line gamma source, which has no source lines above 1001keV. An analysis run with the ORIGEN source model successfully determined a unique solution for both outer radius and source region thickness. The right hand plot of Figure 2 plots the results of the chi-squared error against outer radius and source region thickness for the ORIGEN source model analysis. This solution neglects random Poisson variations of the simulated experimental data.

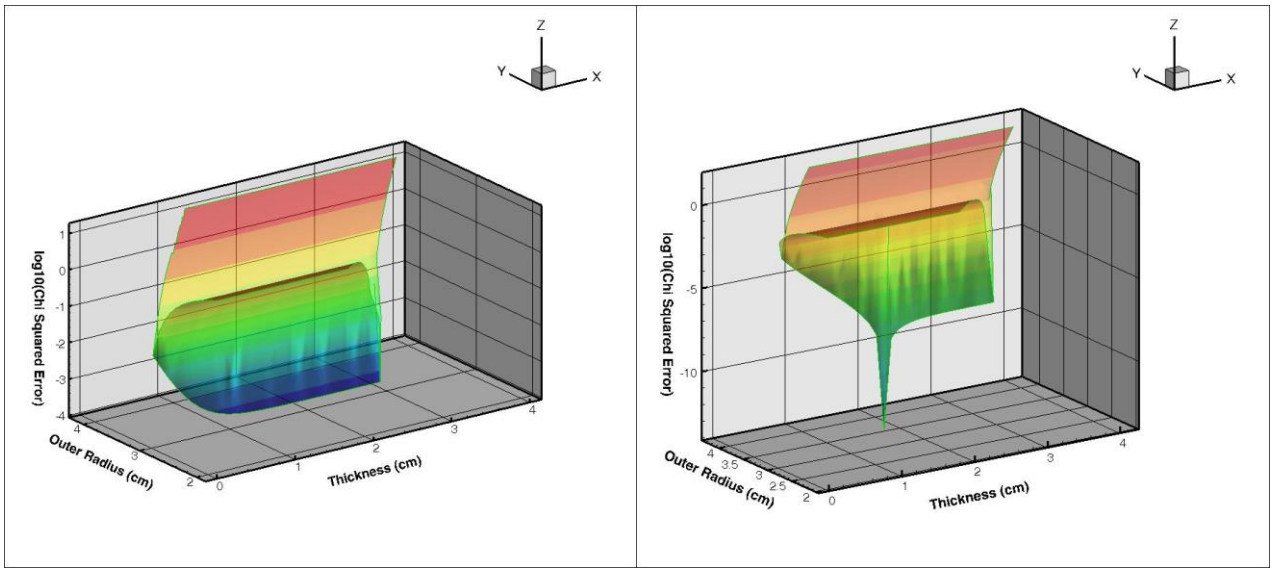

Fig. 2. Log of Chi-Squared Error vs. Outer Radius and Thickness from Least Square Optimization – (left) using source model of 4 gamma lines, and (right) ORIGEN source model.

MESH ADAPTIVE DIRECT SEARCH (MADS)

The exhaustive searches that characterize the problem solutions shown in Figure 2 require significant computational time. Each plot of Figure 2 represents approximately 10 hours of calculations and 900 data points in 0.1cm increments of outer radius and thickness. A Mesh Adaptive Direct Search (MADS) was next used as an alternative to characterize the solution at a lower computational cost. The open source code NOMAD [11] was used as the optimization tool. The NOMAD executable passed parameters to a user created "black box" executable, in this case a Python script that calculated the chi-squared error between the uncollided flux at the detector as calculated by the ray-trace application at the chosen parameters, and the MCNP generated simulated experimental data. The NOMAD solver modifies the parameters of outer radius and source region thickness to minimize the chi-squared error. Based on the previous chi-squared error result, NOMAD will select new parameter values on an interval (the mesh), attempting to minimize the analysis error. As the error decreases the mesh size is decreased from coarse to fine to minimize the calculated error. Results showed that while NOMAD consistently determined the outer radius, it was unable to determine a unique value for the source region thickness. Table I provides results of determinations of source thickness from several NOMAD runs, based on the starting guess that was input, using the 4-line source described above. The NOMAD determination of the minimum chi-squared error value varied randomly with the starting guess values for outer radius and thickness. The final run used the actual values for outer radius and thickness as starting guesses and did not determine the correct source region thickness. NOMAD runs determined a minimum error value and were unable to improve on the error value, stopping where they first reached the minimum. The left hand plot of Figure 3 shows a trace of the NOMAD problem solution with chi-squared error plotted against the values calculated for outer radius and source region thickness. The solution points are color coded by the iteration number of the solution, with the red colors representing the latest points calculated as the solution converged, and corresponding to the minimum error. Similar to the exhaustive search, multiple solutions with equal minimum errors were obtained for the source region thickness.

Table 2. MADS Determined Source Region Thickness

Initial Guess		Nomad Solution
Outer Radius	Thickness	Thickness
1.00	0.00	2.896
2.00	0.00	2.106
3.00	0.00	3.051
3.00	1.00	1.499
4.00	2.00	2.695
5.00	3.00	3.036
3.15	1.55	2.330

The 1245 line ORIGEN source was modeled in the analysis, and NOMAD was able to determine a unique minimum chi-squared error. The right hand plot of Figure 3 graphically shows the NOMAD solution run with the ORIGEN source model. Starting guess values for the ORIGEN source model run were an outer radius of 3.0cm and thickness of 0.0cm. NOMAD calculated values for outer radius and thickness of 3.12cm and 1.58cm respectively, compared to the actual values of 3.15cm and 1.60cm. Calculation time was approximately 100 minutes in both cases, compared to the 10 hour exhaustive search.

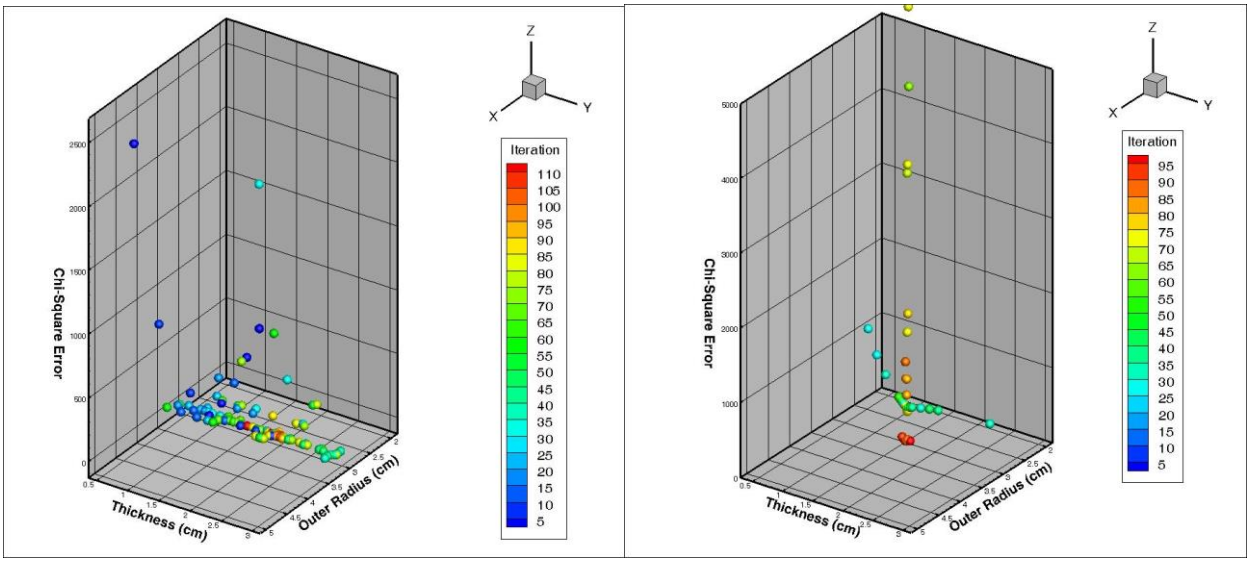

Fig. 2. NOMAD solution of outer radius and thickness with (left) the 4-line source model, and (right) the ORIGEN source model. Solution points are color-coded by iteration number of the solution.

Later analyses added a calculation of the Compton continuum to the analysis models. The Compton continuum was calculated by GADRAS (GAmma Detector Response and Analysis Software) [12]. GADRAS uses a calculation of the Klein-Nishina scattering cross section to compute the Compton continuum. Detector descriptions can be specified so that GADRAS calculates a Compton continuum as it would be seen from the response to a detector type (for example HPGe or NaI detectors). The results of these analyses showed that the addition of the Compton continuum along with the ORIGEN source model did not improve the solution over the ORIGEN source model alone.

RANDOM POISSON VARIATION OF EXPERIMENTAL DATA

While these analyses showed that a constrained solution for the sphere parameters could be obtained by the addition of a more detailed source, the gamma leakage data measured at the detector of the simulated experimental data did not contain Poisson distributed noise. They do not represent data that would be encountered in a field-type environment. In an actual application, the experimental data would include random Poisson distributed noise. GADRAS includes the capability to

calculate the Compton continuum and include the effects of Poisson variation of the data. This feature was used to create simulated experimental data by running the python optimization routine with the actual values of the outer radius and source region thickness, using the ORIGEN generated source and a GADRAS calculated Compton continuum, with the addition of random Poisson noise. The python optimization routine was then run to perform an exhaustive search of the solution for values of outer radius and source region by incrementally varying the outer radius and source region thickness. The incremental calculated data did not contain random variations. Chi-squared error was calculated by comparing the leakage at a detector point calculated at the incremental outer radius and source region thickness to the simulated experimental data. The chi-squared formula of Equation (1) was used with the exception that simulated experimental data was not calculated by MCNP5, but by the python script. In a separate analysis, NOMAD was utilized to directly solve for the values of outer radius and thickness, using the same analysis model and simulated experimental data using the ORIGEN source and GADRAS generated Poisson distributed noise. In Figure 4 below, the left hand plot shows the results from the exhaustive search. While the outer radius is clearly defined, the source region thickness is a continuum of equally valid solutions. The right hand plot of Figure 4 graphically shows the results of the NOMAD analyses. The results of the NOMAD analysis also show that the outer radius was clearly defined, however, many values for source region thickness were calculated with equal minimum error. Both analysis runs were run with the detector counting time for the simulated experimental data set to 1000 seconds. Further analysis runs were performed using increasing values for the counting time to generate the simulated experimental data. Only with excessive counting times (approximately 1 week of continuous counting), could a unique solution for the value of the source region thickness be obtained.

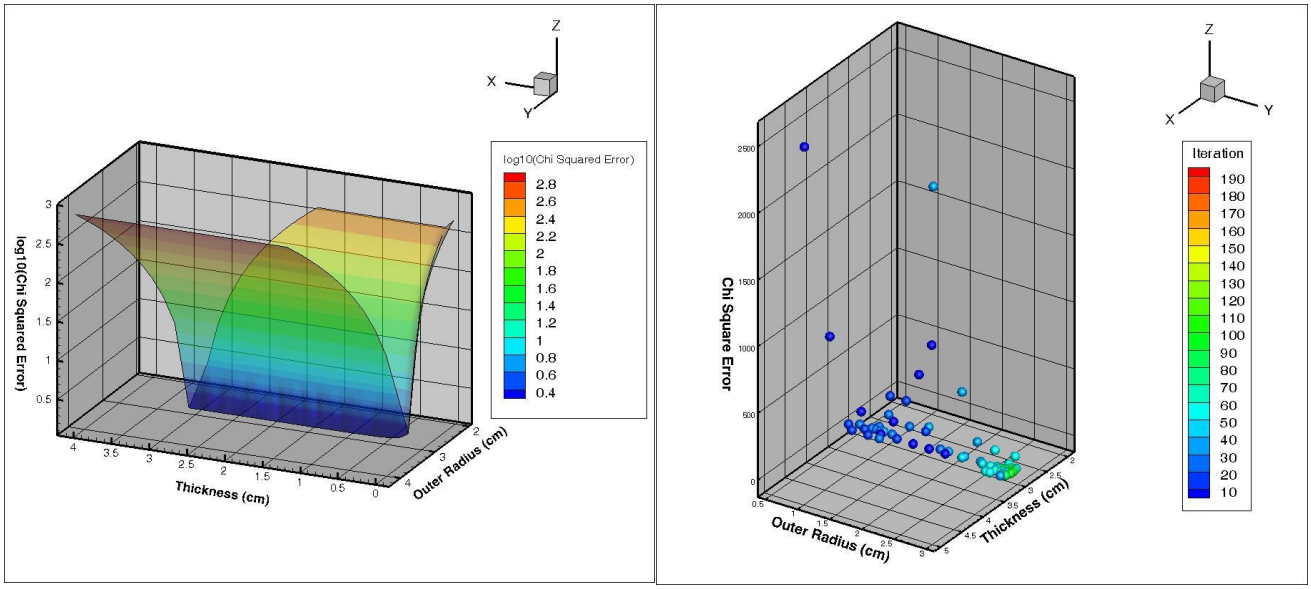

Fig. 4. Exhaustive search (left) and NOMAD solution (right) of outer radius and thickness with an ORIGEN source, Compton continuum generated by GADRAS, with Poisson random sample noise, and 1000 sec count time.

MARKOV CHAIN MONTE CARLO

In an inverse problem, using Bayesian parameter estimation techniques, parameters are assumed to be random variables with a probability density. The probability density may incorporate known data about the solution or may be assumed if not known (for example, a normal distribution, or uniform distribution). The solution to the problem is the posterior density distribution (the density distributions of parameter values) that best matches calculated data for the analysis problem to the observed data distribution.

Equation (2) is Bayes Theorem of Inverse Problems [13]:

$$\pi(q|v_{obs}) = \frac{\pi(v_{obs}|q)\pi_0(q)}{\pi(v_{obs})} \quad (2)$$

where:

π *is a probability density*

$q =$ *a set of parameter values*

$v_{obs} =$ *the observed data based on parameters*

$\pi(q|v_{obs}) =$ *the posterior density(parameter value distribution corresponding to observed data)*

$\pi_0(q) =$ *the prior density(prior value of parameters)*

$\pi(v_{obs}) =$ *the observed data distribution*

$\pi(v_{obs}|q) =$ *the likelihood of observing data values* v_{obs} *given parameter values* q

Markov Chain Monte Carlo (MCMC) techniques may be used to evaluate the posterior density distributions for problems with multiple variable parameters to reduce solution time compared to a Monte Carlo random sampling method. Unlike ordinary Monte Carlo where each sample is independent of all others, in a Markov Chain if the probability of future states of the process depends on the immediately previous state, but only on the one immediately previous state (X_{n+1} depends only on X_n). This can be shown mathematically as [13]:

$$P(X_{n+1} = x_{n+1} \mid X_0 = x_0, \dots, X_n = x_n) = P(X_{n+1} = x_{n+1} \mid X_n = x_n), \quad (3)$$
$$where\ x_i is\ the\ state\ of\ the\ chain\ at\ i$$

Parameter values are varied using one of several algorithms for selection of the next set of variable values based on the result of the previous iteration and the new parameters are used to calculate the new posterior density.

PyMC Implementation

One implementation of Markov Chain Monte Carlo is pyMC [14]. pyMC is set of Python modules and classes that implements Bayesian statistical modeling and analysis capabilities and includes Markov Chain Monte Carlo. To analyze a problem using pyMC, two python scripts are created. The first is the problem calculation. Stochastic variables are declared for the problem parameters, to be varied in discrete increments. A deterministic variable is declared, which is the calculated function at the selected stochastic variable values. This python routine returns the posterior distribution of the problem variables given the prior distribution (initially uniform over inner and outer radius) and the likelihood of the computed response, given the observed response. pyMC updates the stochastic variables using the Metropolis-Hastings algorithm for succeeding iterations. The Metropolis-Hastings algorithm selects the next set of parameter values based on whether the previous set made the error value smaller or larger. If smaller the next parameter value is accepted with a probability of 1. If larger the next parameter is accepted with a reduced probability. The number of iterations is user specified in a second calling script, along with other controls and calls to diagnostic and plotting routines.

The LLNL sphere problem was run in pyMC by creating a python routine, using the ray trace program used for the previously described analyses, to determine leakage at a detector. The source model used was the four gamma lines source from enriched uranium at 144keV, 186keV, 766keV and 1001keV. Stochastic variables for the inner radius and outer radius were defined with minimum and maximum limits, and a deterministic variable "newleakage" which is the leakage at the detector calculated from the current state of the stochastic variables, was defined. Stochastic variables limits were declared as given in Table 2.

Table 2 – pyMC Stochastic Variable Definitions

Variable	Minimum(cm)	Maximum(cm)
Inner Radius	0.0	Outer Radius
Outer Radius	0.1	5.0

Note that as specified the inner radius maximum is the current value of outer radius, preventing non-physical geometry. Plots of the probability densities of the calculated values of outer radius and inner radius are shown below in Figure 5. The results showed that while a converged value for the outer radius can be calculated, the inner radius, shown by the right hand

histogram in Figure 5 below, exhibits a continuum of solutions below approximately 2.75cm inner radius (or approximately 0.4cm source region thickness) down to 0.0cm inner radius (a solid sphere). Below 2.75cm all values for inner radius have approximately equal probability. This is consistent with the results that were obtained using the exhaustive search and NOMAD.

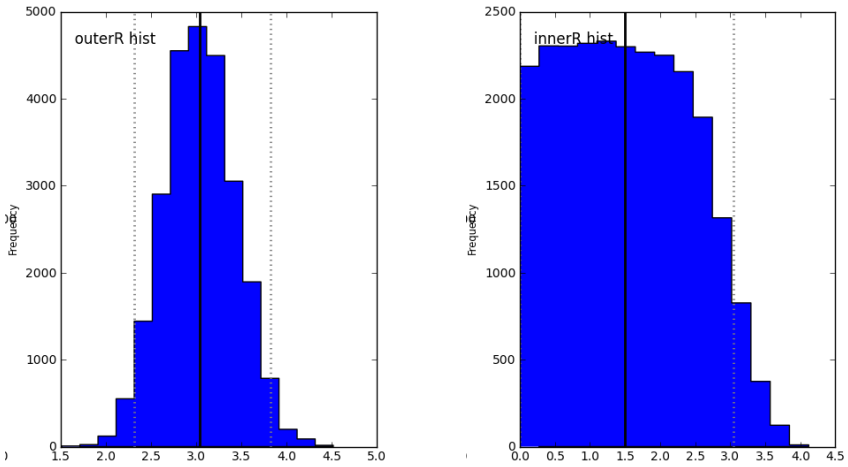

Fig. 5. Inner Radius (left) and Outer Radius (right) probability distributions from pyMC using a 4-line source and 50,000 iterations

The results shown in Figure 5 used raw values for gamma leakage at the detector. Since the intensity of the two higher gammas (766keV and 1001keV) in highly enriched uranium is approximately three orders of magnitude less than the intensity of the two lower energy gammas (144keV and 186keV), the solution is not sensitive to these gamma lines. The 766keV and 1001keV are more penetrating and they could potentially provide a more constrained value for inner radius if their contribution to the solution were higher. To improve the contribution from all four of the gamma lines, the gamma line intensities were normalized by their simulated experimental data leakage. The analysis was re-run with 50,000 iterations. In the right hand plot of Figure 7 below the inner radius is slightly more defined than in Figure 5, however, it is still only possible to determine that inner radius could be approximately 2.0cm or less, as values for inner radius less than approximately 2.0cm have approximately equal probability.

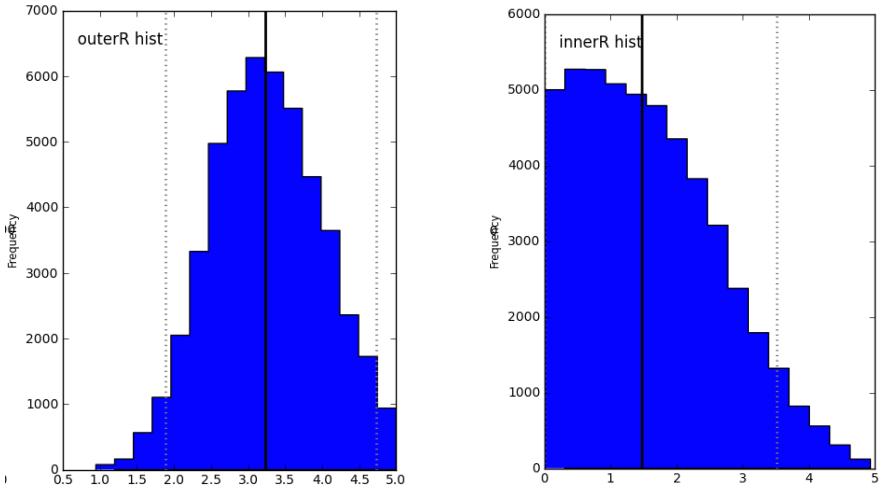

Fig. 7 - Inner Radius (left) and Outer Radius (right) probability distributions from pyMC using a 4-line source, Poisson distribution spectrum, and 50,000 iterations, with normalized leakage

CONCLUSIONS

While the parameters of HEU sources with solid geometry can be reliably determined for values of outer radius using uncollided flux measurements, the addition of more complicated geometry such as a hollow central region leads to solutions where outer radius can be reliably determined, but little information can be determined about source region thickness. This is due primarily to the effect of self-shielding of the uranium gamma lines, especially for the predominant low energy gammas in the LLNL HEU sphere. Few uncollided gammas arrive at the detector from deep inside the source region. The addition of a more detailed source model, in this case generated from ORIGEN, improved the estimate of source region thickness in a model with no random experimental noise in the data. Addition of a calculated Compton continuum did not provide greater fidelity in the solution above that provided by the detailed ORIGEN source model. When random Poisson variations are added to the experimental data, the inverse analysis can no longer determine a unique solution for the source region thickness without unrealistic (approximately 1 week) experimental counting time. The use of pyMC proved to be a useful tool by providing graphical output of the solution parameters and diagnostic tools to examine solution convergence, however no improvement in the solution definition has so far been shown.

ACKNOWLEDGEMENTS

This work was supported by the National Nuclear Security Administration Office of Nonproliferation and Verification Research and Development.

REFERENCES

1. J. FAVORITE, "Using the Schwinger Variational Functional for the Solution of Inverse Transport Problems," *Nuclear Science and Engineering*, **146**, 51-70 (2004).
2. K. BLEDSOE, J. FAVORITE, T. ALDEMIR, "Using the Levenberg-Marquardt Method for Solutions of Inverse Transport Problems in One- and Two- Dimensional Geometries", *Nuclear Technology*, **176**, 106-126 (2011)
3. J. MATTINGLY, D. J. MITCHELL, and L. T. HARDING, "Experimental Validation of a Coupled Neutron-Photon Inverse Radiation Transport Solver," *Nuclear Instruments and Methods in Physics Research A* **652**(1), 537-539, (2011)
4. J. MATTINGLY and D. J. MITCHELL, "A Framework for the Solution of Inverse Radiation Transport Problems," *Transactions on Nuclear Science* **57**(6), 3734-3743 (2010)
5. D. ANDERSON and J. MATTINGLY, "Inverse Radiation Transport Problem Stability Analysis**",** ANS Transactions, **109**(1), 2312-2315 (2013)
6. J. FAVORITE, K. BLEDSOE, D. KETCHESON, "Surface and Volume Integrals of Uncollided Adjoint Fluxes and Forward-Adjoint Flux Products" *Nuclear Science and Engineering*, **163,** 73-84 (2009)
7. W. WEBSTER, C. WONG, "Measurements of the Neutron Emission Spectra from Spheres of N, O, W, EXP, U-235, Exp U-238 and Exp Pu-239 Pulsed by 14Mev Neutrons," California University, Livermore, LL Laboratories (1976).
8. Numpy and Scipy Documentation, SciPy v0.12 Reference Guide (DRAFT), http://docs.scipy.org/doc
9. M.J. Berger, J.H. Hubbell, S.M. Seltzer, J. Chang, J.S. Coursey, R. Sukumar, D.S. Zucker, and K. Olsen, NIST XCOM Photon Cross Section Database, **"**NIST Standard Reference Database 8 (XGAM)", http://www.nist.gov/pml/data/xcom/
10. SCALE: *A Modular Code System for Performaing Standardized Computer Analyses for Licensing Evaluations*, ORNL/TM-2005/39, Version 6, Vols I-III, January 2009. Available from Radiation Safety Information Computational Cneter at Oak Ridge National Laboratory as CCC-750.
11. S. Le DIGABEL, C. TRIBES, C. AUDET, NOMAD User Guide Version 3.6.1, Technical Report G-2009-37, Les cahiers du GERAD, 2009.
12. D. MITCHELL, H. SANGER, K. MARLOW, "Gamma Ray Response Functions for Scintillation and Semiconductor Detectors", Nuclear Instruments and Methods in Physics Research, A276(1989), 547-556.
13. R. C. SMITH, *Uncertainty Quantification, Theory, Implementation and Applications*, Society for Industrial and Applied Mathematics (2014), ISBN 978-1-611973-21-1
14. PyMC, Release 2.1, *PyMC User Guide*, A. Patil, D. Huard, C. Fonnesbeck, J. Slavatier, http:// http://pymc-devs.github.io/pymc/